SYNTHESIS AND CHARACTERIZATION OF UNDOPED AND Mg-DOPED ZnO NANORODS BY HYDROTHERMAL METHOD FOR PHOTODETECTOR AND LED APPLICATIONS

by

SHROOK ADNAN AZZEZ

Thesis submitted in fulfillment of the requirements

for the degree of

Doctor of Philosophy

November 2017

ACKNOWLEDGEMENT

I would like to express my gratitude for the guidance and support from my main advisor, Professor Dr. Zainuriah Hassan during the course of my Ph.D. research. She is an extremely helpful and encouraging advisor, who helped me through difficult times in my research work. I would also like to express my appreciation to my co-supervisor Dr. Jalal Jabbar Hassan for his guidance and support throughout my study. I would like to express my deepest thanks to my friend, Mohamed Saleh for his help and excellent cooperation to achieve our research. Many thanks to all my friends and colleagues especially Dr. Rawnaq and Dr. Nezar who supported me and helped me at the School of Physics in Universiti Sains Malaysia. In addition, I offer my appreciation to School of Physics and N.O.R. lab staff: Dr. Naser, Ee Bee Choo, Mohd Anas, Yushamdan, Abdul Jamil, Mohtar, Shahil, Syed and Ong Ching Hin, for their technical assistance and I am totally indebted to the wonderful help. I am greatly indebted to my colleagues at Ministry of Science and Technology of Iraq for their continued encouragement to me. A special thanks to my family. Words can't express how grateful I am to my mother, sisters and all my uncles, aunts, cousins for their unconditional love and support. I would never have got anywhere near this level without such a great family. Last, and most important, my deepest and heartfelt gratitude goes to my husband for his continued support and encouragement during the period of the study.

Shrook A. Azzez

November 2017

Penang, Malaysia.

TABLE OF CONTENTS

ACKNOWLEDGEMENT ..... **ii**

TABLE OF CONTENTS ..... **iii**

LIST OF TABLES ..... **vii**

LIST OF FIGURES ..... **viii**

LIST OF SYMBOLS ..... **xi**

LIST OF ABBREVIATIONS ..... **xii**

ABSTRAK ..... **xiii**

ABSTRACT ..... **xv**

CHAPTER 1: INTRODUCTION **1**

1.1 Introduction 1

1.2 Motivation and problem statement 3

1.3 Research objectives 4

1.4 Originality of thesis 5

1.5 Scope of the study 5

1.6 Thesis outline 6

CHAPTER 2: BACKGROUND AND LITERATURE REVIEW **7**

2.1 Introduction 7

2.2 Nanomaterials 7

2.3 ZnO and ZnO nanorods 9

2.4 Structural properties 10

2.5 Optical properties of ZnO 11

2.6 Native defects of ZnO 13

2.7 Mg-doped ZnO nanorods 15

2.8 Growth mechanism of undoped and Mg-doped ZnO nanorods by drothermal deposition method 18

2.9 Literature review 21

2.9.1 Undoped ZnO nanorods 21

2.9.2 Doping of ZnO nanorods 22

2.9.3 Mg-doped ZnO nanorods 24

2.10 Optoelectronic device principle 30
2.10.1 Photodiodes 33
2.10.1(a) Overview of photodiodes 33
2.10.1(b) Undoped and Mg-doped ZnO UV detectors 36
2.10.2 Light emitting diodes 40
2.10.2(a) Overview 40
2.10.2(b) Undoped and Mg-doped ZnO-based LEDs 42

CHAPTER 3: EXPERIMENTAL AND CHARACTERIZATION TOOLS..... 46

3.1 Introduction 46
3.2 Growth of undoped ZnO nanorods 46
3.2.1 Substrate cleaning 46
3.2.2 Preparation of ZnO seed layer 48
3.2.3 Thermal annealing process 49
3.2.4 Hydrothermal synthesis of the ZnO nanorods 50
3.2.5 Synthesis of Mg-doped ZnO nanorods by hydrothermal method 51
3.3 Characterization tools 52
3.3.1 Field emission scanning electron microscope (FESEM) and energy dispersive X-ray spectrometer (EDX) 53
3.3.2 X-ray diffraction (XRD) 54
3.3.3 Band gap measurements 55
3.3.4 Optical characterization 57
3.4 Device fabrication and characterization techniques 59
3.4.1 Fabrication of undoped and Mg-doped n-ZnO/p-Si HJ PDs 59
3.4.2 Fabrication of undoped and Mg-doped n-ZnO/p-GaN HJ LEDs 60
3.5 Electrical characterization 61
3.6 Electroluminescence measurements 61

CHAPTER 4: RESULTS AND DISCUSSION FOR UNDOPED ZnO NANORODS ON p-Si AND p-GaN SUBSTRATES..... 63

4.1 Introduction 63
4.2 Effect of the annealing of seed layer on the growth of the ZnO nanorods 63
4.2.1 Surface morphology 63
4.2.2 Crystal structure 67
4.2.3 Raman Spectroscopy 69

4.3 Effect of variation precursor concentrations on the growth of undoped ZnO nanorods on Si substrates ……70
4.3.1 Surface morphology 70
4.3.2 Crystalline structure 73
4.3.3 Optical properties 76
4.3.3(a) Raman spectra 76
4.3.3(b) UV-Vis diffuse reflectance spectra 77
4.3.3(c) PL spectra 79
4.4 Undoped ZnO NRs on a p-GaN substrate…….. 80
4.4.1 Surface morphology 80
4.4.2 Crystalline structure 81
4.4.3 Optical properties 83
4.4.3(a) Raman spectrum 83
4.4.3(b) PL spectra 83
4.5 Summary ……. 84

CHAPTER 5: RESULTS AND DISCUSSION FOR Mg-DOPED ZnO NANORODS ON p-Si AND p-GaN SUBSTRATES..... 86

5.1 Introduction ……. 86
5.2 Effect of growth temperature on the synthesis of Mg-doped ZnO nanorods on Si substrates …… 87
5.2.1 Surface morphology 87
5.2.2 Crystalline structure 89
5.2.3 Optical properties 93
5.2.3(a) Raman spectra 93
5.2.3(b) UV-Vis DR spectra 94
5.2.3(c) PL spectra 95
5.3 Effect of Mg concentrations in growth of Mg-doped ZnO NRs on Si substrate …….. 97
5.3.1 Surface morphology 97
5.3.2 Crystalline structure 102
5.3.3 Optical properties 104
5.3.3(a) Raman spectra 104
5.3.3(b) UV-Vis DR spectra 105
5.3.3(c) PL spectra 108
5.4 Mg-doped ZnO NRs on p-GaN substrates ……110

5.4.1 Surface morphology 110
5.4.2 Crystalline structure 111
5.4.3 Optical properties 112
5.4.3(a) Raman spectrum 112
5.4.3(b) PL spectrum 113
5.5 Summary 114

CHAPTER 6: RESULTS AND DISCUSSION FOR PHOTODETECTOR AND LIGHT EMITTING DIODE APPLICATIONS 116

6.1 Introduction 116
6.2 Undoped and Mg-doped ZnO NRs based HJ PD 117
6.3 Undoped and Mg-doped ZnO-based HJ LEDs 124
6.4 Summary 131

CHAPTER 7: CONCLUSION AND FUTURE WORK 132

7.1 Conclusion 132
7.2 Future work 134

REFERENCES 135

APPENDICES

LIST OF PUBLICATIONS

LIST OF TABLES

Page

Table 2.1: Summary of LED devices with their electrical and EL properties as well as the structure and methodology. 44

Table 4.1: Structural parameters of ZnO NRs synthesized under different precursor concentrations. 76

Table 5.1: Structural parameters of Mg-doped ZnO NRs synthesized at different growth doping temperatures. 92

Table 5.2: Structural parameters of Mg-doped ZnO NRs synthesized under different dopant concentrations. 104

Table 6.1: Electrical properties for the fabricated n-ZnO/p-Si and n-ZnO:Mg/p-Si in comparison with other reported ZnO-based PDs. 123

Table 6.2: Comparison of the characteristic parameters of undoped and doped n-ZnO/p-GaN LEDs. 127

LIST OF FIGURES

Page

Figure 2.1: Common forms of ZnO 1-D nanostructures. 9

Figure 2.2: (a) The B4 structure and (b) B4 unit cell of ZnO. 11

Figure 2.3: Schematic band diagram of the DLE emissions in ZnO 13

Figure 2.4: Native defects in crystal materials. 14

Figure 2.5: Schematic of the energy band diagram in (a) ZnO and (b) Mg-doped ZnO. 18

Figure 2.6: (a) The FESEM image of the Mg- doped ZnO NRs at Mg/ Zn = 1, (b) the XRD pattern of this sample. 27

Figure 2.7: Band diagram of a p-n junction at; (a) thermal equilibrium, (b) forward bias and (c) reverse bias. 32

Figure 2.8: Calculation of rise and decay times of a pulse current. 34

Figure 2.9: Schematic of the photoconduction in a ZnO NRs photodetector and energy band diagram (a) under dark condition, and (b) under UV light illumination 35

Figure 2.10: (a) The FESEM image of the prepared ZnO NRs on Si, (b) the PL spectrum of the ZnO NRs, (c) the transient response of photocurrent for the fabricated ZnO/p-Si UV photodiode. 37

Figure 3.1: Flowchart of the fabrication and characterization of UV photodetector and LED based on undoped and Mg-doped ZnO NRs. 47

Figure 3.2: Auto HHV500 magnetron sputtering system. 49

Figure 3.3: The thermal annealing furnace system. 50

Figure 3.4: Schematic of the setup used in synthesizing undoped and Mg-ZnO NRs. 51

Figure 3.5: FESEM type FEI Nova NanoSEM system. 53

Figure 3.6: High-resolution XRD system. 55

Figure 3.7: Carry Series UV-Vis-NIR Spectrophotometer. 56

Figure 3.8: PL and Raman spectroscopy system. 58

Figure 3.9: The schematic of the device for measuring the photocurrent in ZnO NRs. 59

Figure 3.10: Schematic illustration of (a) the heterojunction LED structure, (b) energy band diagram of the n-ZnO/p-GaN heterojunction structure. 60

Figure 3.11: Schematic diagram of the setup for electroluminescence measurement. 62

Figure 4.1: FESEM images of ZnO seed layer at different annealing temperatures (a) 200˚C, (b) 300˚C, (c) 400˚C, and (d) 500˚C. 64

Figure 4.2: XRD patterns of ZnO seed layer at various annealing temperatures. 65

Figure 4.3: FESEM images of ZnO NRs grown on (a) bare Si, plain and cross section view of ZnO-seed layer annealed at different temperatures: (b) and (c) 200˚C, (d) and (e) 300˚C, (f) and (g) 400˚C, and (h) and (i) 500˚C, respectively. 66

Figure 4.4: XRD patterns of the ZnO NRs grown seeded Si substrates after different annealing temperatures. The inset is a schematic of a hexagonal ZnO NR. 68

Figure 4.5: Raman spectra of the ZnO NRs grown on seeded Si substrates after different annealing temperatures. 70

Figure 4.6: Top view and cross section view FESEM images of ZnO NRs grown under different concentration: (a) and (b) at 25 mM; (c) and (d) at 50 mM; (e) and (f) at 75 mM; (g) and (h) at 100 mM. 72

Figure 4.7: EDX spectra of undoped ZnO NRs grown under different concentrations. 74

Figure 4.8: XRD patterns of ZnO NRs grown under different concentrations. 75

Figure 4.9: Raman spectra for ZnO NRs grown under different concentrations. 77

Figure 4.10: (a) Kubelka-Munk diffuse reflectance plot of ZnO NRs grown under different concentrations. (b) The bandgap energy of ZnO NRs grown under different concentrations is found by plotting $(F(R)\ h\nu)^2$ versus $h\nu$. 78

Figure 4.11: PL spectra of ZnO NRs grown under different concentrations. 80

Figure 4.12: 45° tilted-view and cross section (inset) of FESEM image of as-grown ZnO NRs that were obtained at 75 mM precursor onto ZnO seed (pretreated at 400℃) p-GaN substrate. 81

Figure 4.13: XRD pattern of bare GaN substrate and ZnO NRs on p-GaN. 82

Figure 4.14: Raman spectrum of ZnO NRs grown on p-GaN substrate. 83

Figure 4.15: PL spectra for bare p-GaN substrate and n-ZnO/p-GaN heterostructure. 84

Figure 5.1: Low and high magnifications FESEM images of Mg-doped ZnO NRs grown at different growth temperatures: (a) and (b) 130˚C, (c) and (d) 140˚C, (e) and (f) 150˚C, and (g) and (h) 160˚C. 88

Figure 5.2: EDX data of Mg-doped ZnO NRs grown under different temperatures. 90

Figure 5.3: XRD patterns of ZnO:Mg NRs grown at various growth temperatures. 91

Figure 5.4: Raman spectra of Mg-doped ZnO NRs grown at various temperatures. 94

Figure 5.5: (a) Kubelka-Munk diffuse reflectance plot of ZnO:Mg NRs grown at various growth temperatures. (b) The bandgap plot energy of ZnO:Mg NRs grown at different growth temperatures is found by plotting $(F(R)\ h\nu)^2$ versus $h\nu$. 95

Figure 5.6: PL spectra of Mg-doped ZnO NRs grown under different growth temperatures. 96

Figure 5.7: FESEM images of Mg-doped ZnO NRs at different concentration of Mg. 99

Figure 5.8: The EDX spectra of Mg doped ZnO NRs. 101

Figure 5.9: XRD patterns of Mg-doped ZnO NRs on Si substrate. 102

Figure 5.10: Raman spectra of Mg-doped ZnO NRs on Si substrate. 105

Figure 5.11: (a) Kubelka-Munk diffuse reflectance plot of ZnO:Mg NRs grown under various Mg concentrations. (b) the bandgap energy of ZnO:Mg NRs grown under various Mg concentrations is found by plotting $(F(R)\ h\nu)^2$ versus $h\nu$. 107

Figure 5.12: PL spectra of Mg-doped ZnO NRs 109

Figure 5.13: 45° tilted-view and cross section (inset) FESEM image of Mg-doped ZnO NRS grown on p-GaN substrate. 111

Figure 5.14: XRD pattern of Mg-doped ZnO NRs on p-GaN substrate. 112

Figure 5.15: Raman spectrum of Mg-doped ZnO NRs on p-GaN substrate. 113

Figure 5.16: PL spectrum of Mg-doped ZnO NRs on p-GaN substrate. 114

Figure 6.1: I-V characterization of (a) ZnO/Si and (b) ZnO:Mg/Si HJ PDs. 118

Figure 6.2: Semi-logarithmic plot of the current as a function of the bias voltage (I-V) of (a) ZnO/Si and (b) ZnO:Mg/Si HJ PDs. 119

Figure 6.3: The current–time curves of (a) ZnO/Si and (b) ZnO:Mg/Si HJ PDs under on/off switch illumination at 5 V reverse bias voltage. 122

Figure 6.4: I-V characterization of (a) n-ZnO/p-GaN and (b) n-ZnO:Mg/p-GaN HJ LEDs. 125

Figure 6.5: Semi-logarithmic plot of the current as a function of the bias voltage (I-V) of (a) n-ZnO/p-GaN and (b) n-ZnO:Mg/p-GaN HJ LEDs. 126

Figure 6.6: The EL spectra of (a) n-ZnO/p-GaN and (b) n-ZnO:Mg/p-GaN HJ LED devices under various bias voltages. Insets in (a) and (b) are photos taken from the device under an injection current of 20 mA. 129

LIST OF SYMBOLS

T	Absolute temperature
Å	Angstrom
Eg	Band gap
ϕ	Barrier height
K	Boltzmann constant
θ	Bragg's angle
e^-	Charge of electron
h^+	Charge of hole
I	Current
I_d	Dark current
℃	Degree Celsius
q	Electron charge
eV	Electron volt
E_f	Fermi level
I_f/I_r	Rectification ratio
n	Ideality factor
c	Lattice constant
ε_z	Lattice strain
V_o	Oxygen vacancies
I_{ph}	Photocurrent
S	Photosensitivity
hν	Photon energy
I_s	Saturation current
V	Voltage
λ	Wavelength
Zn_i	Zinc interstitials
V_{Zn}	Zinc vacancies

LIST OF ABBREVIATIONS

a.u	Arbitrary unit
I-t	Current-time
I-V	Current-voltage
DL	Deep level
DRS	Diffuse reflectance spectroscopy
EL	Electroluminescence
EDX	Energy dispersive X-ray spectroscopy
FESEM	Field emission scanning electron microscopy
FWHM	Full width at half maximum
HJ	Heterojunction
HTM	Hexamethylenetetramine
JCPD	Joint Committee on Powder Diffraction
LED	Light emitting diode
NR	Nanorod
NBE	Near band edge
PD	Photodetector
PL	Photoluminescence
RCA	Radio Corporation of America (cleaning procedure)
RF	Radio frequency
UV	Ultraviolet
Vis	Visible
B4	Hexagonal wurtzite
XRD	X-ray diffraction

SINTESIS DAN PENCIRIAN NANOROD ZnO YANG TIDAK DIDOP DAN DIDOP DENGAN Mg DENGAN KAEDAH HIDROTERMA UNTUK APLIKASI PENGESAN CAHAYA DAN DIOD PEMANCAR CAHAYA

ABSTRAK

Nanorod (NRs) zink oksida (ZnO) yang tidak didop dan didop dengan Mg mempunyai potensi besar untuk aplikasi dalam bidang peranti optoelektronik. Oleh itu, adalah sangat penting untuk merealisasikan pertumbuhan terkawal bagi NRs ini dan mengkaji sifatnya. Dalam tesis ini, NRs ZnO telah ditumbuhkan di atas p-Si dengan lapisan benih ZnO dan substrat p-GaN menggunakan kaedah hidroterma untuk digunakan dalam pengesan cahaya ultraungu (UV) dan diod pemancar cahaya (LED). Kesan parameter hidroterma termasuk suhu rawatan haba lapisan benih dan kepekatan zink nitrat dan hexamethylenetetramine pada pembentukan ZnO NRs atas substrat p-Si disiasat. Syarat-syarat penyediaan optimum untuk NRs ZnO kemudiannya digunakan untuk menumbuhkan NRs ZnO yang didop dengan Mg (ZnO:Mg) atas substrat p-Si di bawah parameter hidroterma yang berbeza. Larutan bahan permulaan dan magnesium nitrat sebagai pendopan telah digunakan. Suhu tindak balas yang diubahkan dan kepekatan pendopan menggalakkan pembentukan NRS dengan ciri-ciri yang unik. Pada suhu pemendapan 150°C, bentuk piramid tirus satu arah diperolehi bagi NRs ZnO:Mg. Di samping itu, morfologi berevolusi daripada rod heksagon dengan permukaan atas yang rata dan sisi yang licin bagi NRs ZnO kepada rod tirus dan rod dendritik dengan menukar kepekatan bahan pendopan sebanyak 1.15, 3.24, dan 6.06 % at. Mg, masing-masing. NRs dendritik mempunyai keluasan permukaan yang lebih besar untuk peranti optolelektronik yang lebih cekap daripada NRs biasa.

Pengukuran fotoluminesen (PL) menunjukkan bahawa spektrum pancaran daripada NRs ZnO memperlihatkan puncak UV yang berpusat di 384 nm dan jalur cahaya nampak yang lebar sekitar 500-700 nm. Puncak PL bagi ZnO teranjak biru kepada 377, 374, dan 371 nm dengan peningkatan kepekatan dopan Mg sebanyak 1.15, 3.24, dan 6.06 % at., masing-masing, yang menunjukkan bahawa jurang jalur ini telah ditala dengan menggantikan Mg ke dalam kekisi perumah ZnO. Nisbah puncak UV dan cahaya nampak untuk seperti-dendritik ZnO:Mg adalah kira-kira tujuh kali lebih tinggi daripada NRs ZnO, yang menunjukkan bahawa NRs ini mempunyai kualiti optik yang sangat baik. Berdasarkan keadaan pertumbuhan optimum, fotodiod n-ZnO/p-Si dan n-ZnO:Mg/p-Si telah difabrikasikan. Di bawah voltan pincang, NRs seperti-dendritik ZnO:Mg mempamerkan tindak balas yang lebih cepat dengan kepekaan unggul sebanyak 3.96×10^{6}%, yang merupakan tiga kali lebih peka daripada NRs ZnO. Di samping itu, syarat-syarat pertumbuhan ini digunakan untuk mensintesis NRs ZnO dan NRs seperti-dendritik ZnO:Mg pada substrat p-GaN untuk aplikasi LED. Di bawah suntikan arus hadapan, elektroluminesen untuk LED n-ZnO/p-GaN mempamerkan puncak ungu yang tajam berpusat pada 400 nm, manakala elektroluminesen untuk LED n-ZnO:Mg/p-GaN menunjukkan satu anjakan biru menuju ke arah kawasan UV pada 375 nm.

SYNTHESIS AND CHARACTERIZATION OF UNDOPED AND Mg-DOPED ZnO NANORODS BY HYDROTHERMAL METHOD FOR PHOTODETECTOR AND LED APPLICATIONS

ABSTRACT

Undoped and Mg- doped zinc oxide (ZnO) nanorods (NRs) have great potential applications in the fields of optoelectronic devices. Therefore, it is very important to realize the controllable growth of these NRs and investigate their properties. In this dissertation, ZnO NRs were grow on ZnO-seeded p-Si and p-GaN substrates using hydrothermal method for use in ultraviolet (UV) photodetectors and light-emitting diodes (LEDs). The effects of the hydrothermal parameters including the heat-treatment temperature of the seed layer and the zinc nitrate and hexamethylenetetramine precursor concentrations on the formation of ZnO NRs on the p-Si substrate were investigated. The optimum preparation conditions for undoped ZnO NRs were then used to grow Mg-doped ZnO NRs on a p-Si substrate under different hydrothermal parameters. A solution of starting materials and magnesium nitrate as a dopant was used. Varying the reaction temperature and dopant concentration favours the formation of NRs with unique characteristics. The surface morphology, crystallinity, and optical properties of the as-prepared films were systematically investigated. At a deposition temperature of 150°C, unidirectional tapering pyramidal Mg-doped ZnO:Mg NRs were obtained. In addition, the morphology evolved from hexagonal rods with a flat top surface and smooth sides for undoped ZnO NRs to tapered rods and dendritic rods by changing the concentrations of the dopant material to 1.15, 3.24, and 6.06 at. % Mg, respectively. Dendritic NRs

have larger surface areas for more efficient optoelectronic devices than bare NRs. photoluminescence (PL) measurements indicated that the emission spectrum of undoped ZnO NRs covered a UV peak centred at 384 nm and a broad visible band around 500–700 nm. The PL peak of ZnO blue-shifted to 377, 374, and 371 nm with the increasing Mg doping concentrations of 1.15, 3.24, and 6.06 at. %, respectively, which indicated that the band gap was tuned by substituting Mg into the ZnO host lattice. The ratio of the UV to visible peaks for dendritic-like Mg-doped ZnO was approximately seven times higher than that of undoped ZnO NRs, indicating that the ZnO NRs were highly crystallized with excellent optical quality. Based on the optimum growth conditions, n-ZnO/p-Si and n-ZnO:Mg/p-Si heterojunction (HJ) photodiodes were fabricated. Under a reverse bias voltage of 5 V, the dendritic-like Mg-doped ZnO NRs exhibited a faster response with a superior photosensitivity of 3.96×10^{6}, which is three times more sensitive than undoped ZnO NRs. In addition, these growth conditions were used to synthesize undoped and dendritic-like Mg-doped ZnO NRs on a p-GaN substrate for LED applications. Under a forward injection current, the electroluminescence of n-ZnO/p-GaN HJ LED exhibited a sharp violet peak centred at 400 nm and a broad, weak visible peak extending from 490 to 590 nm, while the electroluminescence of n-ZnO:Mg/p-GaN LED showed a blue shift toward the UV region and a unique peak centered at 375 nm.

CHAPTER 1: INTRODUCTION

1.1 Introduction

ZnO has caught the attention of many researchers in the field of ultraviolet (UV) optoelectronic devices, especially light-emitting diodes (LEDs) and photodetectors, due to its excellent physical and chemical properties. It is attractive for its useful characteristics such as its wide direct band gap (3.37 eV), large excitonic binding energy (60 meV, which makes excitons stable above room temperature), high thermal and chemical stability, low cost, non-toxicity, high radiation resistance, wide availability, and simple fabrication process requirements [1–3]. ZnO is used in a wide range of applications, such as in medicine, as a pigment in UV-protective paints, as an additive for rubber and plastics, in heat-resistant glass, and in spacecraft protective coatings [4, 5]. Furthermore, ZnO exhibits a diverse range of nanostructures such as nanowires, nanorods (NRs), nanotubes, nanoflowers, nanoribbons, and nanobelts. These nanostructures offer advantages for applications in various kinds of nanoscale functional devices such as UV-blue semiconductor lasers [6], flat panel displays [7], solar cells [8], and gas sensors [9].

Another very important aspect of ZnO as a semiconductor material is the possibility of controlling its band gap and thus influencing its physical, chemical, and electronic properties by doping. Its ionicity is between that of covalent and ionic compounds (the Zn–O bonds are half ionic and half covalent), thereby making doping ZnO much easier than doping other covalently bonded wide-band-gap semiconductors [10, 11]. Therefore, its direct band gap can be modulated by doping with many elements, such as Cd, S, In, Mn, and Mg [12–16]. Among them, Mg can be easily

doped into the ZnO lattice to enlarge the band gap without affecting the crystal structure because of its similar radius with that of Zn, thus avoiding the formation of large lattice distortion [17]. Band gap tuning by incorporating Mg in ZnO layers is an important step in designing ZnO-based optoelectronic devices to finely tune the colour of LEDs, to create barrier layers in order to confine carriers in the heterojunction (HJ) devices, as well to fabricate high-speed UV detectors with different cut-off wavelengths [18–20].

The morphology of Mg-doped ZnO (ZnO:Mg) nanostructures could be tuned from flower-like [21], needle-like [22], urchin-like [23] or dendritic structures [24] by hydrothermal, wet chemical precipitation, chemical vapour deposition, and physical–chemical vapour deposition methods, respectively. These morphologies all exhibit a high surface area-to-volume ratio, which means that this material can be classified among new materials with potential applications in many fields of nanotechnology. In particular, dendritic-like nanostructures, as they have long main trunks and parallel secondary branches with sharp edges or tips, are particularly popular because of their unique geometrical and electronic characteristics, which can provide specific surface area and direct charge carrier transport pathway in both the trunks and branches, similar to the efficient transport of water and carbohydrates in natural trees resulting from their fractal geometry. Therefore, investigating the ability of Mg doping to improve the structural and optical properties of ZnO for the fabrication of high-quality photodetectors and light-emitting devices is a worthwhile research area.

1.2 Motivation and problem statement

Low-dimensional ZnO nanostructures occupy a special place among wide-band-gap semiconductors, which have been widely studied due to their multifunctional applications in electronic, optoelectronic, piezoelectric, and biomedical science. Particularly, the optoelectronic device applications of one-dimensional (1D) ZnO NRs have recently become a major focus of nanoscience research because of an increased need for solid-state light sources and detectors operating in UV spectral ranges in the nanometre regime. Vertically aligned ZnO NRs have received particular attention due to their potential to enhance the performance of these applications thanks to their unique electrical and optical properties.

A major drawback of ZnO is the fact that it is very rich in oxygen vacancy defects [25]. These defects (which bring energy levels within the band gap) induce band gap narrowing [26, 27] and forming recombination centre traps [5, 28], which greatly affect the crystallinity and thus limit device performance. For example, in the case of photoconductivity, traps reduce the lifetime of carriers in the bands; these traps retain electrons for a long time, resulting in slow response and recovery behavior [28, 29]. In the case of photo-emission, traps function as non-radiative emission or deep level (DL) emission centers, which can substantially quench the exciton-related near-band-edge (NBE) emission [31, 32] .

Removing these defects that hinder the development of efficient ZnO-based optoelectronic devices remains a great challenge. The hypothesis is to reduce these defects and improve the structural and optical quality of ZnO NRs by thermal annealing at appropriate temperature and/or under suitable environments. However, at

high annealing temperature under oxygen environment, oxidation-induced stacking falts and void defects related to incorporation of oxygen which occupies interstitial position will occur. Doping and alloying are also used by some research groups to improve the quality of ZnO. Indeed, Mg is an excellent dopant for eliminating these defects in the crystal lattice, increasing the band gap energy, and hence improving the UV emission intensity without changing the crystal structure of ZnO [33–35], since the ionic radius of the Mg ion (0.57 Å) is very similar to that of the Zn ion (0.60 Å) [36]. ZnO:Mg NRs have mostly been fabricated using vapour phase deposition techniques. Although perfect-quality ZnO:Mg NRs have been successfully obtained from the vapour phase, these techniques have some disadvantageous process requirements that still need to be resolved such as high temperature, high vacuum, high energy, sophisticated equipment, and rigid experimental conditions. In contrast, the hydrothermal method is simpler than the vapour phase deposition; it operates at low temperature, it is lower in cost due to its use of water as a reaction medium, it does not require a complex vacuum system, it offers a large yield, and more importantly, its process parameters are controllable.

1.3 Research objectives

The main objectives of this study can be summarized by the following points:

1. To synthesize n- type undoped and Mg-doped ZnO NRs on p- type Si and GaN substrates by the hydrothermal method under different growth conditions and characterize the fabricated NRs to study their effects on the structural and optical properties using SEM, XRD, Raman, UV-VIS DR and PL spectra.

2. To fabricate p–n junction diodes for UV photodetector and light emitting diode based on undoped and Mg-doped ZnO NRs and to study their photodetection and luminescence properties, respectively.

1.4 Originality of thesis

The originality of this thesis can be summarized by the following points:

1. The growth of highly oriented, aligned, and ordered NRs of n- ZnO with uniform length and diameter on p- Si and p-GaN substrates.
2. The synthesis of dendritic-like Mg-doped ZnO NRs on p- Si and p-GaN substrates by a hydrothermal method.
3. A UV photodetector was fabricated based on a dendritic-like n-ZnO:Mg NRs/p-Si-based HJ, exhibiting superior photosensitivity and a fast photoresponse.
4. A UV LED was fabricated based on the dendritic n-ZnO:Mg NRs/p-GaN HJ.

1.5 Scope of the study

This work focused on the synthesis of undoped and Mg-doped ZnO NRs fabricated by a hydrothermal method at different growth conditions. The parameters were optimized to control the surface morphology, crystal structure, and optical properties of ZnO NRs after doping with Mg. Then, the Mg-doped ZnO NRs with the optimal properties were used to fabricate superior-photosensitivity p–n junction PDs. Undoped and Mg-doped ZnO NRs LEDs with a controllable wavelength were fabricated.

1.6 Thesis outline

Chapter 1 includes a brief overview of ZnO NRs, the motivations and problem statements, the objective of the study, and the originality of this thesis.

Chapter 2 presents a literature review, the theoretical background of growth technique for undoped and Mg-doped ZnO NRs, and UV photodetector and LED applications.

Chapter 3 describes the methodology and instrumentation used to characterize undoped and Mg-doped ZnO NRs and device applications.

Chapter 4 presents and discusses an analysis of the properties of ZnO NRs on Si substrates with different seed layer annealing temperatures and precursor concentrations in the starting solution. The characterization of ZnO NRs fabricated on a p-GaN substrate is also discussed in this chapter.

In **Chapter 5**, the effects of growth temperatures and dopant concentrations on the morphology, structural, and optical properties of the hydrothermally grown ZnO:Mg NRs are presented and discussed. The characterization of ZnO:Mg NRs synthesized on a p-GaN substrate is also presented.

Chapter 6 reports the results of UV detection achieved by PDs based on p–n junctions using n-ZnO NRs/p-Si and n-ZnO:Mg NRs/p-Si. In addition, the controllable light emission achieved by p–n junction n-ZnO NRs/p-GaN and n-ZnO:Mg NRs/p-GaN LEDs is presented.

Finally, **Chapter 7** presents conclusions and areas for future research.

CHAPTER 2: BACKGROUND AND LITERATURE REVIEW

2.1 Introduction

With the development of nanotechnology, optoelectronic devices based on a nanostructure have attracted considerable attention because these nanostructure-based optoelectronic devices often exhibit favourable properties over other materials, such as their simple synthesis conditions, high crystallinity, and the potential for nanoscale device integration. In this chapter, types of nanomaterials are described for a general understanding of the nanomaterials used in this study. Next, the structural properties and optical features of ZnO nanomaterials will be briefly addressed. Then, a literature review will be presented concerning the hydrothermal preparation of undoped and Mg-doped ZnO NRs. A part of this section is devoted to reviewing the use of undoped and Mg-doped ZnO NRs in UV photodetectors and LEDs as well as the theoretical background of these optoelectronics applications.

2.2 Nanomaterials

Nanotechnology is the design and application of nanoscale materials, which exhibit fundamentally new properties and functions relative to those of bulk materials. Nanomaterials are defined as engineered materials with a least one nanoscale dimension in the range of 1–100 nm. Nanomaterials are classified according to their nanoscale dimensions into four types: 0-dimensional (nanoparticles and quantum dots, etc.), 1-dimensional (1-D) (NRs, nanowires, nanotubes, nanobelts), 2-dimensional (thin films and nanosheets), and 3-dimensional (nanospheres). The index number (0, 1, 2, 3) refers to the number of dimensions smaller than 100 nm.

When the size of materials is reduced to the nanoscale range, unique physical, electrical, and optical properties emerge as a result of the surface-area-to-volume ratio and quantum confinement effects [37, 38]. The surface-to-volume ratio increases as the particle size decreases, which means that the number of surface atoms increases relative to the bulk, and hence, these materials are more reactive than their bulk counterparts. In particular, 1-D nanostructure materials have received increasing attention due to their potential as building blocks for other 2 and 3-dimentional architectures [39], which are of considerable interest for nanomaterial applications in optoelectronic devices, especially devices that require certain orientations and perfectly single-crystalline structures, such as LEDs, laser diodes, and PDs [40, 41].

The size of the 1-D nanostructure is quantified using the aspect ratio, which is the ratio of the length to the diameter. A schematic of the common forms of 1-D nanomaterials is illustrated as Figure 2.1. Nanowires and nanobelts have good aspect ratio, but may lack uniformity in their morphology that is characterized by curvatures or bends [42]. Nanotubes also exhibit a high aspect ratio (with respect to both their outer and inner diameters) and uniform morphology, but their hollow morphology leads to poor top contacts (on the borders areas only). In contrast, their non-hollow counterparts, i.e., NRs, have attracted extensive interest for use as nanoscale building blocks in advanced optoelectronic devices, since they have high-quality single crystals, well-faceted edges and corner morphology, offer a higher aspect ratio, and good electrical contact due to the flat top surface of the NRs, as well as they provide charge carriers with a direct transport pathway to the electrode [43, 44]. In addition, vertically

oriented NRs offer an excellent material architecture because of their unique ability to decrease grain boundaries, disorder, and discontinuous interfaces [45, 46].

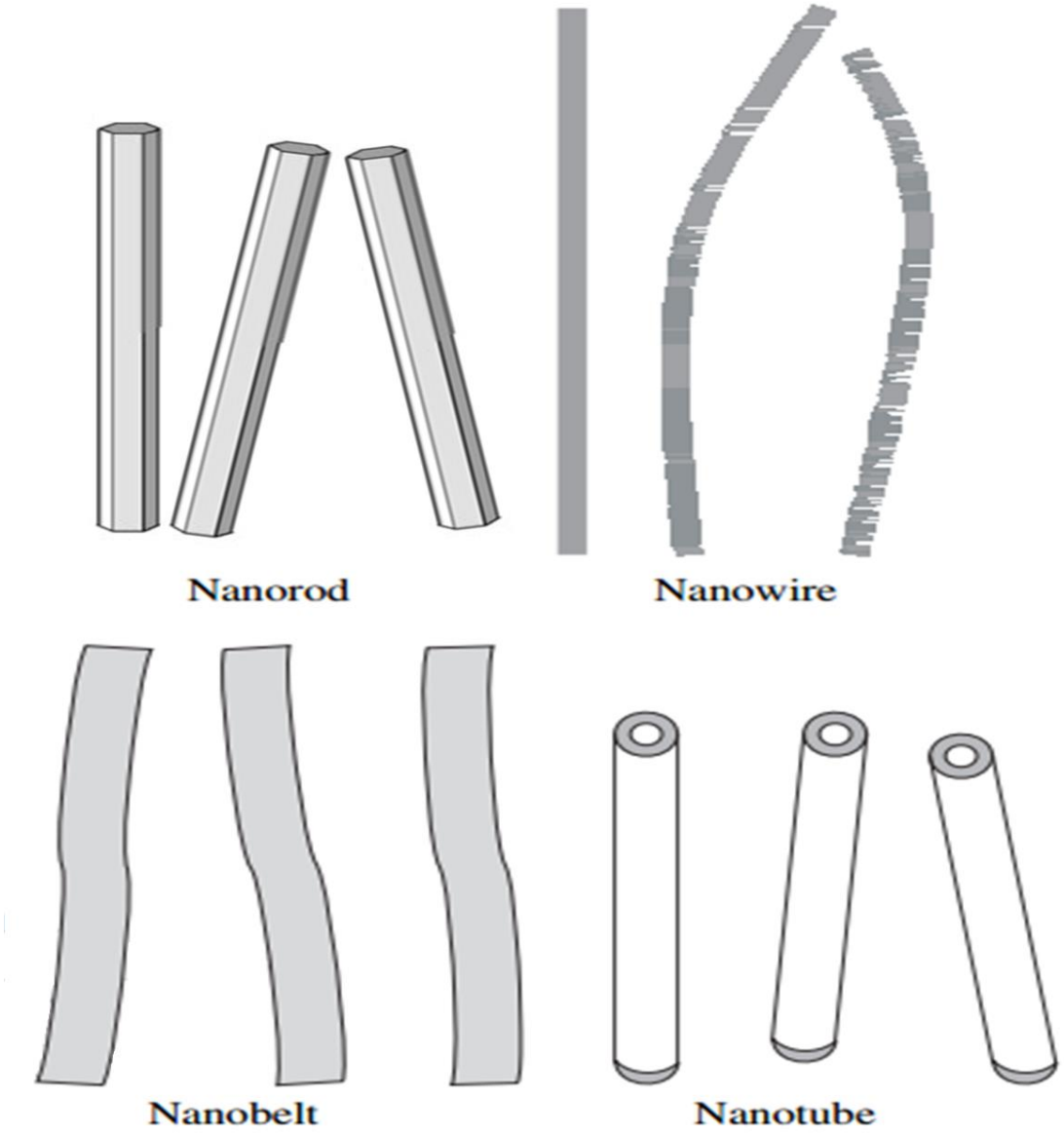

Figure 2.1: Common forms of ZnO 1-D nanostructures [42].

2.3 ZnO and ZnO nanorods

ZnO is a promising II-VI compound semiconductor because of its excellent optical, electronic, and chemical properties. It has a direct wide band gap energy of 3.37 eV that makes it a good candidate for short wavelength devices such as LEDs and

laser diodes. ZnO is transparent to visible light, which gives it some potential applications in solar cells [47]. In addition to its unique chemical and thermal properties, ZnO also has piezoelectric and photoconductive characteristics. Because of these properties, ZnO has been demonstrated to have many practical applications such as in biomedical and chemical sensors, piezoelectric transducers, and transparent conductors. ZnO can be grown on inexpensive substrates such as Si at a relatively low temperature. In addition, it can also be synthesized in numerous nanostructure forms such as nanocombs, nanorings, nanosprings, nanobows, nanohelixes, nanoflowers, nanoneedles, nanobelts, NRs, and nanotubes [48].

Among all these forms, ZnO NRs have very important features; a very large surface-to-volume ratio, high optical gain, fast response, and specific crystalline orientation, which are of interest for developing next-generation high-performance nanodevices [49]. In many cases, these NRs display a degree of crystal perfection that far exceeds that of thin films, even on lattice-mismatched surfaces.

2.4 Structural properties

ZnO crystallizes in two main forms: hexagonal wurtzite (B4) and the zincblende (B3) structure, wherein each Zn atom is surrounded by four O atoms situated at the corner of a tetrahedron and vice versa [50]. B4 ZnO is more stable phase at ambient temperature and pressure than the zincblende structure. It consists of multiple planes of tetrahedrally coordinated O^{2-} and Zn^{2+} ions arranged alternatingly along the c-direction, thus providing two polar charges along the structure. The surfaces can be terminated with either Zn^{2+} or O^{2-}, which leads ZnO to possess positive or negative charges on its surfaces. The B4 ZnO has a hexagonal unit cell with two lattice

parameters, a and c, which are 3.2535 Å and 5.2151 Å (JCPS card No. 01-080-0074), respectively. The axial ratio c/a is about 1.602, which is slightly different from the ideal value for a hexagonal cell c/a = 1.633 (in response to strain or stress) [50, 51]. Figure 2.2 shows a schematic representation of the B4 ZnO structure.

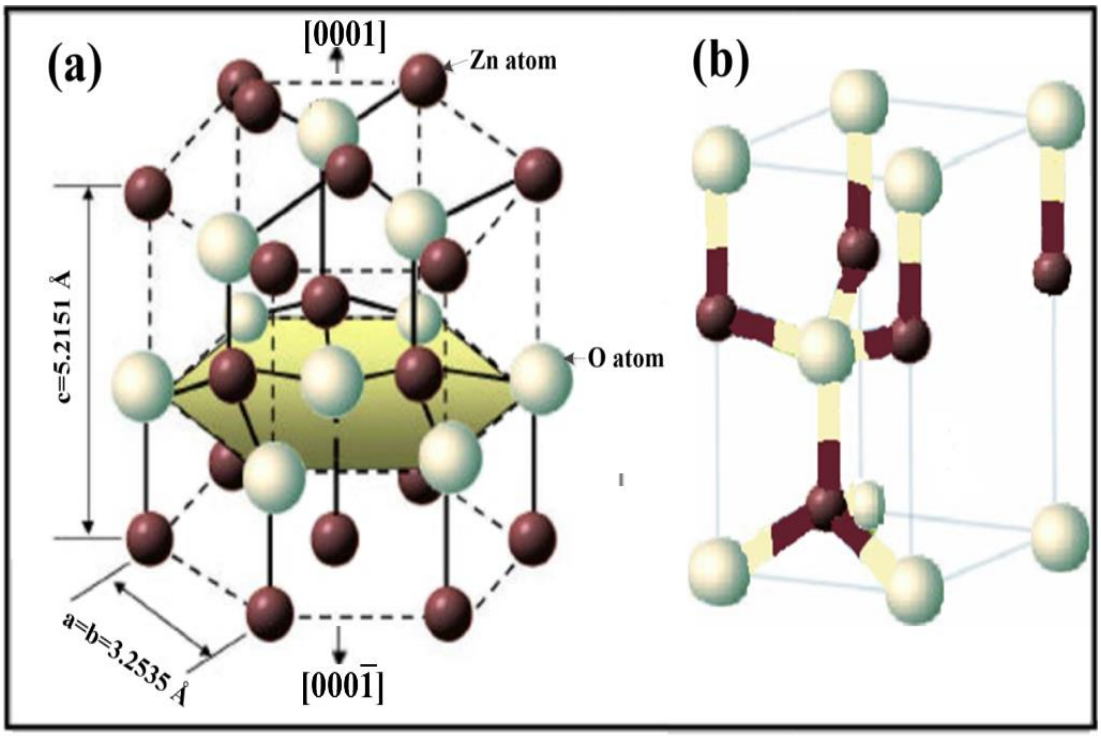

Figure 2.2: (a) The B4 structure and (b) B4 unit cell of ZnO [52].

2.5 Optical properties of ZnO

The optical properties of semiconductor materials are associated with intrinsic and extrinsic effects. The intrinsic optical transition occurs between electrons in conduction band and holes in the valence band, resulting in excitons (electron–hole pair) due to the Coulomb interaction. Extrinsic effects are related to dopants or defects, which usually create discrete electronic states between the valence and conduction bands.

The optical transitions in ZnO can be determined by several experimental techniques such as absorption, reflection, transmission, and photoluminescence (PL) spectroscopy techniques. Among them, PL spectroscopy has been widely used to study the optical properties of ZnO nanostructures, and it provides information on the band gap, defects, and crystallinity. Generally, the PL spectra of ZnO nanostructures show two emission bands; one is a sharp emission centred in the UV region (around 380 nm) corresponding to NBE emission of direct exciton recombination [53] and the other is a broadband emission positioned in the visible region corresponding to DL emission, which is attributed to the intrinsic (native) defects of ZnO, such as oxygen vacancies (V_o), Zn vacancies (V_{Zn}), Zn interstitials (Zn_i), and oxygen interstitials (O_i), which generate sub-band levels inside the band gap [54, 55].

Therefore, several different visible regions appear, i.e., violet, blue, green, yellow, and red emission in the range of 395, 405-450, 500-580, 600, and 700-750 nm, respectively [56, 57]. The violet emission is due to the transition of electron just below the conduction band to valence band, but it is not NBE [58]. Blue emission in ZnO is attributed to zinc vacancies due to the electron transition from the Zn_i energy level (at ~0.22 eV below conduction band) to the local V_{Zn} level [58, 59]. The green emission is the most commonly observed defect emission in ZnO nanostructures [40, 60, 61], which is attributed to the V_o defects [62–64]. In general, oxygen vacancies exhibit three types of charge states, namely, singly ionized, doubly ionized, and neutral oxygen vacancies [65]. The green emission is the result of the recombination of the photogenerated electron from conduction band or Zn_i with the deeply trapped hole in single ionized V_o^+ [56, 66–68]. The yellow emission is attributed to the transitions of

photogenerated electron close to the conduction band to the deeply trapped hole in the single negatively charged Oi [66, 67]. The red emission is attributed to the combination of emissions related to the doubly ionized V_o^{++} and O_i^- [69]. Figure 2.3 shows the schematic band diagram of the DL emission in ZnO.

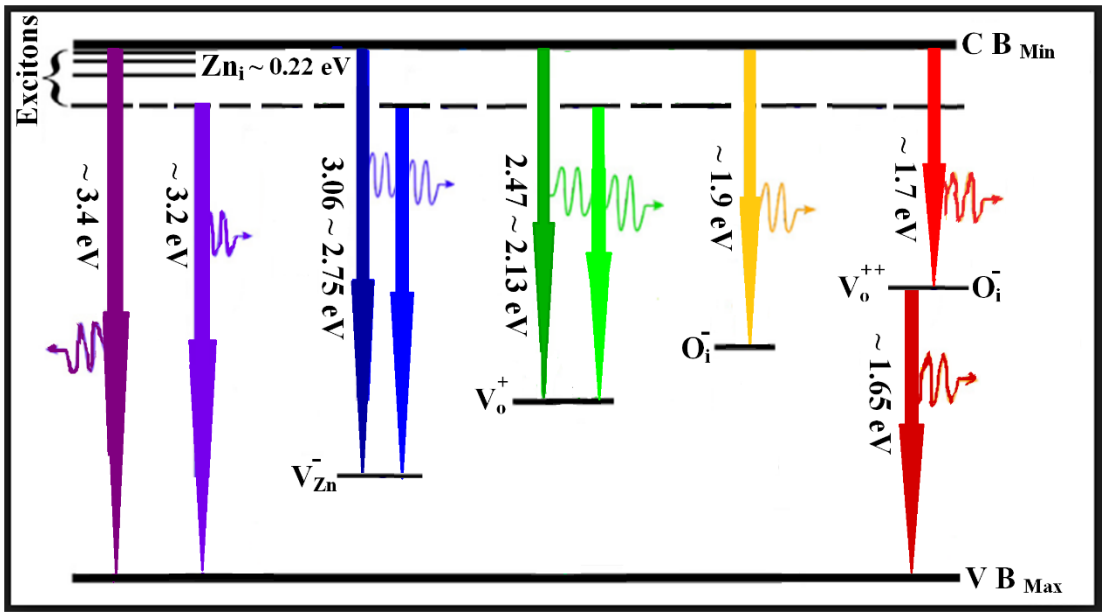

Figure 2.3: Schematic band diagram of the DL emissions in ZnO (adapted from Ref. [56])

In high-quality ZnO NRs with low defect concentrations, only UV emission has been observed; the position of this PL peak shifts toward longer or shorter wavelengths depending on intrinsic defects or extrinsic dopants. The ratio of the NBE emission peak to that of deep level emission peak (NBE/DL) characterizes the quality of ZnO. For ZnO NRs, a high NBE/DL ratio means a lower concentration of the DL defects and hence excellent crystallinity and good optical properties [69].

2.6 Native defects of ZnO

Native or intrinsic defects are imperfections in the crystal lattice that exist in almost all crystals, among which vacancies (i.e., missing atoms at regular lattice

positions) and interstitials (i.e., extra atoms occupying interstices in the lattice) are the most common defects, as shown in Figure 2.4. The concentration of a point defect is given by $C=N_{sites}$ exp $(-E_f /KT)$ where E_f is the formation energy, N_{sites} is the number of sites the defect can be incorporated on, K is the Boltzmann constant, and T the temperature [55]. Defects significantly influence the electrical and optical properties of a semiconductor.

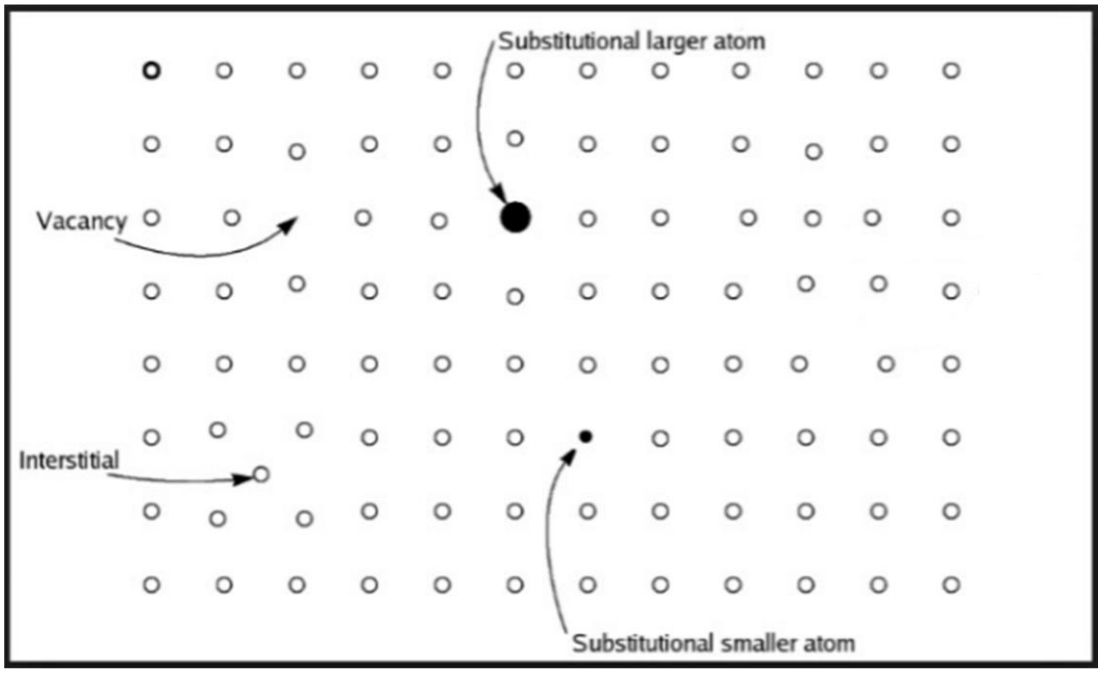

Figure 2.4: Native defects in crystal materials.

As mentioned in the previous section, ZnO has native defects during the deposition process such as V_O, V_{Zn}, and Zn_i. Notably, B4 ZnO is naturally an n-type semiconductor [70]. There is some argument over what is the main reason for this n-type behaviour. It has long been accepted that V_o and/or Zn_i act as shallow donors, and the unintentional n-type conductivity of ZnO is due to these defects [71]. However, recent studies on high-quality ZnO crystals have demonstrated that this hypothesis may not be correct [55, 72]. It has been confirmed that the V_o are actually deep rather than

shallow donors and thus do not contribute to the n-type conductivity of ZnO, while Zn_i defects are shallow donors, which would contribute to the native n-type conductivity in as-grown ZnO crystals [54, 55, 73, 74]. The radius of Zn (0.74 Å) is much smaller than that of O (1.32 Å) [51], which enables Zn interstitials to form more easily, and the n-type character of ZnO is intrinsically due to Zn interstitials. Meanwhile, V_{Zn} are shallow acceptors, which play a role in the p-type conductivity of ZnO [75].

2.7 Mg-doped ZnO nanorods

The doping of a semiconductor is defined as the process of adding a small amount of foreign atoms called dopants into its crystal lattice with the intent of producing changes in its properties; when a sufficiently large amount of dopant atoms are involved, this process is referred to as alloying. Many conditions are required for the doping process: (1) The dopant atom must be placed in the same position as that of the semiconductor atom (i.e., substitution). (2) There should be no distortion in the crystal after the addition of the dopants. (3) The size of the dopants should be nearly the same as that of the original atom in the crystal.

ZnO NRs exhibit novel physical properties that make them interesting candidates for nanoscale optoelectronic devices. To enhance the electrical and optical properties of ZnO as well as make these devices highly stable during operation, doping with suitable elements has been the preferred approach [76]. ZnO can be doped in four principal ways , i.e., doping with: (1) donor impurities (e.g., B, Al, Ga, In, Cl, Br, Ti, etc.) to achieve n-type conductivity, (2) acceptor impurities (e.g., P, As, Sb, Na, K, Ag, etc.) to achieve p-type conductivity, (3) rare-earth elements (Eu, Nd, Sm, Tb) to achieve the desired optical properties, and (4) transition metals (V, Mn, Fe, Co, and

Ni) to achieve the desired magnetic properties. Doping of ZnO with different donors (Mg and Be) broadened the UV emission peak and it also shifted according to the type of doping element [77].

Mg is the most common dopant for ZnO since the ionic radius of Mg^{2+} (0.57 Å) is very similar to that of Zn^{2+} (0.60 Å) [35], which means that replacing Zn with Mg will not significantly distort the lattice [17, 78]. Moreover, it retains a single phase wurtzite structure of ZnO [79]. The Mg content modulate the value of the optical band gap of ZnO; meanwhile, by alloying ZnO with MgO to obtained the ZnMgO ternary system, the band gap can be turned from 3.3 to 4 eV [70, 79–81]. Moreover, the incorporation of Mg in the ZnO NRs results in a decrease in the V_o density due to the stronger Mg–O bonding than that of Zn–O, indicating that Mg serves as an excellent absorber for the emission from these defects in ZnO NRs [82, 83]. Ogawa *et al.* [84] and Karthick and Vijayalakshmi [83] reported that the incorporation of Mg into ZnO tends to decrease the amounts of oxygen vacancies that cause the green PL in ZnO.

Therefore, doping ZnO with Mg enables a stable formation of the excitons, thus enhancing the UV luminescence intensity and resulting in wide-band-gap materials [35,79,85]. This is important for fabricating high-performance UV LEDs and laser diodes, which is useful for many semiconductor device applications. For example, it can greatly increase data storage density and kill bacteria [86, 87]. Furthermore, ZnMgO exhibits strong absorption in the UV region, which demonstrates its potential for highly sensitive UV photodetectors to detect high-temperature burning [88]. In addition, more UV light can penetrate through ZnMgO than through ZnO due to its larger band gap, which is suitable for UV-transparent top electrodes in UV light

sensors, UV LEDs, as well as some types of solar cells [89, 90]. Adding Mg can lead to more thermally stable ZnMgO [91]. Moreover, ZnMgO alloy is an important barrier material for realizing the highly efficient UV light emission [92].

The optical band gap in ZnO is defined as the minimum energy needed to excite an electron from the valance band to the conduction band. The optical gap equals the energy separation Eg_0 between the band edges, as shown for the case of isotopic and parabolic bands in Figure 2.5 (a). When ZnO is doped with Mg, the Mg^{+2} ions may be substituted with Zn^{+2} or occupy the interstitial position. The substitution of both ions does not supply an additional free electron because both have a valence of 2+. The existence of Mg ions in the interstitial position gives them opportunity to act as donor. Thus, the interstitial Mg ions cause an additional free electron and the increase in the carrier concentration; hence there is further increase in the n-type nature of ZnO. These donor electrons occupy the bottom states of the conduction band and the optical transitions are vertical because the Pauli Exclusion Principle prevents states from being doubly occupied. In fact, the optical gap is given by the energy difference between states with Fermi momentum in the conduction and valance bands as shown Figure 2.5 (b). Consequently, the measured band gap determined from the onset of inter-band absorption moves to a higher energy (i.e., undergoes "a blue shift") and the band gap increases as the carrier concentration increases.

The solubility of Mg in the structure of B4 ZnO is an important issue, and it is limited by the technique used for the deposition [93]. The solubility of Mg in B4 ZnO without phase segregation has been reported to be ~4 at.% [35, 94]. At higher Mg concentrations, ZnMgO films result with a metastable cubic phase due to the phase

separation of MgO, which is an important research problem. It has been claimed that using a vapour phase route such as pulsed laser deposition enables incorporating up to ~40 at.% Mg [35]. However, the study of Mg-doped ZnO NRs synthesized at low temperatures is important to create new forms of this material, which could open more avenues for its applications.

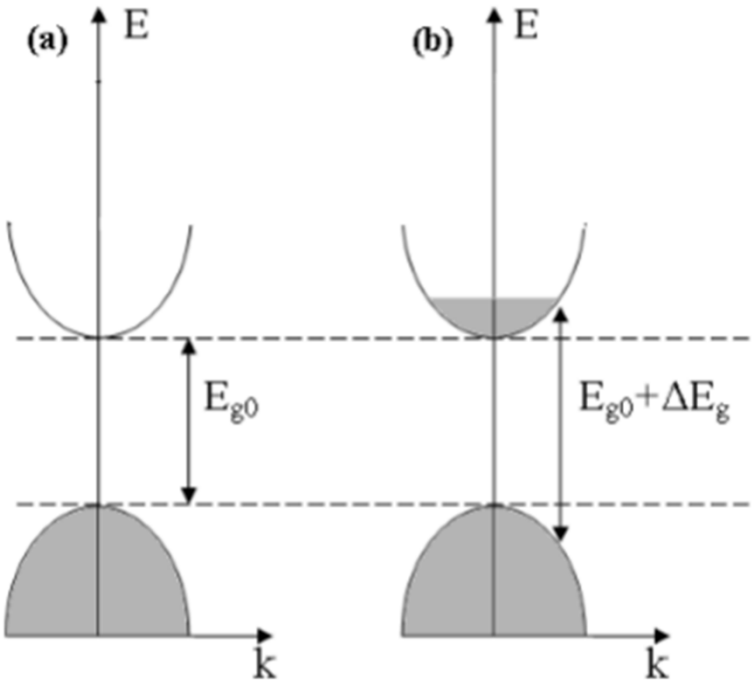

Figure 2.5: Schematic of the energy band diagram in (a) ZnO and (b) Mg-doped ZnO

2.8 Growth mechanism of undoped and Mg-doped ZnO nanorods by hydrothermal deposition method

Several techniques have been explored to successfully fabricate undoped and Mg-doped ZnO NRs, which can be classified into vapour phase and solution phase techniques. The vapour phase technique includes thermal evaporation, chemical vapour deposition, metal organic chemical vapour deposition, pulsed laser deposition, radio frequency (RF) sputtering, and molecular beam epitaxy. These techniques produce high-quality Mg-doped ZnO NRs under well-controlled, high-vacuum

conditions, but they are limited because of their high temperature and pressure requirements, expensive equipment, complexity, intense energy requirements, substrate choice, and low product yield.

In contrast, solution phase techniques including solvothermal and hydrothermal methods have many advantages such as simplicity, low cost, easy handling, large-scale production, environmental friendliness, greater choice of substrates, as well as good control of the morphology and composition. The solvothermal method involves a chemical reaction in the presence of organic or inorganic solvent (non-aqueous) such as methanol, ethanol, and propanol at high temperatures (e.g., 400°C) and pressure. Meanwhile, the hydrothermal method is very versatile for the synthesis of 1-D nanophase materials; it is a process of chemical reactions between precursors in the presence of an aqueous solution in a sealed reaction system (e.g., a Teflon-lined stainless steel autoclave); the temperature of the reaction system should be higher than the boiling temperature of water and autogenous pressure in order to afford a new crude yield. The main advantages of the hydrothermal method are: (a) the reactions occur at relatively lower temperatures (25–200°C) than those in the vapour phase (>450°C), which may be useful for in situ doping during the synthesis of ZnO NRs; (b) it does not use metal catalysts. Instead, a high quality seed layer is required to initiate the growth; (c) single crystals are obtained; (d) no harmful solvents are required, and thus, the process is safe and cost-effective thanks to the use of water as a reaction medium; and (e) pollution is diminished because of the closed system conditions.

Generally, to form a solid phase from solution, nucleation and growth are the basic processes for the hydrothermal method. Nucleation sites play a crucial role in governing the morphology, growth density, and orientation of ZnO NRs because they can decrease the lattice mismatch between the surface substrate and the crystal nuclei to form NRs, thus improving the orientation, distribution, and morphology of ZnO NRs [95–97]. On the other hand, the molecular chemical reaction plays a crucial role in the phase evolution of the final crystallites by modifying the nucleation and crystal growth steps to obtain the desired morphology and nanostructure size [98]. In this study, a substrate is immersed vertically in an autoclave containing a heated solution of $Zn(NO_3)_2 \cdot 6H_2O$ and $Mg(NO_3)_2 \cdot 6H_2O$ that act as sources of Zn^{2+} and Mg^{2+}, respectively, with hexamethylenetetramine (HMT) as the OH^- source. A number of chemical reactions are involved in the overall process, as summarized by the following chemical equations [99]:

$$C_6H_{12}N_4 + 6H_2O \rightarrow 6HCHO + 4NH_3 \quad (2.1)$$

$$NH_3 + H_2O \rightarrow NH_4^+ + OH^- \quad (2.2)$$

$$Zn(NO_3)_2 \rightarrow Zn^{2+} + 2NO_3^- \quad (2.3)$$

$$Zn^{2+} + 2OH^- \rightarrow Zn(OH)_2 \quad (2.4)$$

$$Zn(OH)_2^- \rightarrow ZnO + H_2O \quad (2.5)$$

$$nZnO + xMg \rightarrow (ZnO)n\text{-}x\text{:}Mg + xZn \quad (2.6)$$

The above chemical equations demonstrate that at the early stage of reaction, HMT nuclei begin to hydrolyse in water and gradually produce ammonia and OH^-, as

described in Eq. (2.1) and (2.2). The concentration of OH^- ions is important in the precipitation of Zn hydroxide ($Zn(OH)_2$) nuclei in aqueous solution (Eq. (2.4). Meanwhile, ammonia provides a basic environment for the formation of $Zn(OH)_2$ [100], which is subsequently dehydrated to generate ZnO nuclei on the substrate (Eq. (2.5)). These ZnO nuclei are the initial building blocks for the formation of the final ZnO NRs. During the doping process, Mg ions are released from the Mg nitrate hydrates and are easily incorporated into the ZnO lattice by substituting Zn ions because their ionic radii are nearly equivalent and because Mg is more chemically reactive with O than Zn, thus producing Mg-doped ZnO NRs [101], as shown in Eq. (2.6).

2.9 Literature review

2.9.1 Undoped ZnO nanorods

The low-temperature fabrication of hydrothermal ZnO NRs generally introduces enormous amounts of defects, e.g. V_o. These defects produce potential wells that can trap and affect the movement of carriers and degrade device performances [102]. Therefore, several research studies have been conducted to prepare the high-quality ZnO NRs using thermal annealing or doping to suppress oxygen vacancies.

Lee *et al.* studied the effects of post-annealing at 400°C for 1 h in oxygen or forming gas (H_2:N_2 1:9) on the optical properties of ZnO NRs [103]. The result indicated that the increase in the ratio of UV to visible emission of ZnO NRs annealed in oxygen could be attributed to the reduced concentration of the oxygen defects. The value of NBE/DL was approximately 2.5.

Ridhuan *et al.* investigated the effect of heat-treatment temperature (250–450℃ for 10 min in air) of ZnO seeds deposited on Si substrate by RF magnetron sputtering [45]. They observed that the ZnO NRs which were grown from the ZnO seed layer annealed at 400°C exhibited a strong UV emission peak and low, deep-level emission peak. The obtained results reveal that deep-level emission remain, resulting from the radiative recombination of a photogenerated hole with an electron occupying an V_o. Chen *et al.* have reported similar results for ZnO nanowires with improved crystallinity and a reduced concentration of V_o through annealing in O_2 at 800°C for 60 min [104].

Recently, Dogar *et al.* investigated the effects of high temperature rapid thermal annealing (range from 600 to 900℃) for the ZnO seed layers on the optical properties of ZnO NRs [105]. The PL analyses revealed that the ZnO NRs grown on ZnO seed annealed at 900°C demonstrated strong UV to visible emission. However, this high annealing temperature can limit future applications of ZnO NRs because it degrades the ZnO seed layer.

2.9.2 Doping of ZnO nanorods

Many research groups have focused on improving the optical quality of hydrothermally grown ZnO NRs by reducing defects and modulating the band gap by doping. Chen *et al.* fabricated undoped and Al-doped ZnO nanostructures on ZnO-seeded ITO substrates [106]. Various ZnO morphologies resulted from the introduction of the Al dopant. After the sample was doped with 1 at.% Al, a more intense UV emission and a lower DL emission appeared compared to those of the undoped sample, indicating that the ZnO NRs were better crystallized with less Al doping.

Kumar *et al.* systematically investigated the influence of Mn doping on the structural and optical properties of ZnO NRs [107]. X-ray diffraction (XRD) results demonstrated that the products were well crystallized. The energy band gap of undoped ZnO was around 3.1 eV, which red shifted to 2.7 eV after doping with Mn. The optical analysis showed a significant suppression in the DL emission of the Mn-doped systems. The ratio NBE/DL increased to 6.1 because of the decrease in the oxygen-related defects and the enhanced crystallinity of the Mn-substituted ZnO species.

Lee *et al.* fabricated highly oriented ZnO NRs and F-doped samples on a sol–gel-seeded FTO substrate [25]. They found that the rod-shaped arrays of ZnO were transformed into taper-shaped arrays at a high concentration of F. The XRD results showed a negligible shift in the 2θ of the (002) peak because of the relatively similar ionic radii between F and O, which indicated that there was no severe distortion in the ZnO lattice after doping with F. The PL results revealed a suppression of the intrinsic defects in ZnO lattice via F^- incorporation by annihilating V_o and substituting F at the lattice O sites. The current–voltage (I–V) characteristics of the corresponding photovoltaic device showed an improvement correlated with the defect-passivation effect of the F dopants, which inhibited the charge trapping phenomenon at ZnO DL defect states and increased the carrier mobility of the devices.

Zhang *et al.* successfully controlled the morphology of ZnO single-crystal NRs after doping with Cd for acetone gas sensors [108]. The tips of the hexagonal ZnO NRs changed from planar to hexagonal pyramids after doping. The Cd-doped ZnO NRs exhibited higher crystallinity than the pure ZnO NRs.

2.9.3 Mg-doped ZnO nanorods

To date, some studies have been reported on controlling various hydrothermal parameters such as the dopant ion concentration, annealing conditions, seed layer, and substrate properties for the fabrication of Mg-doped ZnO NRs. However, no report has studied the effects of the growth temperature on the characteristics of ZnO NRs doped with Mg via the hydrothermal method.

Fang *et al.* investigated the effect of the Mg doping concentration on ZnO NRs grown on ZnO-seeded ITO substrates by the aqueous solution method [109]. They found that ZnO:Mg NRs were uniformly distributed across the entire substrate and that the tops of the NRs were hexagonal, with the c-axis perpendicular to the substrate surface. ZnO:Mg NRs with various sizes were obtained during the growth of NRs with different Mg doping concentrations. The energy-dispersive X-ray spectroscopy (EDX) results confirmed that with 3.36×10^{-2} mM Zn and 0.00, 2.67×10^{-4}, 8.00×10^{-4}, and 13.33×10^{-4} mM Mg precursor aqueous solution concentrations, the final concentrations of Mg in the as-grown samples were 0.00, 0.21, 0.35, and 0.45 wt.%, while those of Zn were 74.32, 75.04, 79.47, and 77.26 wt.%, and those of O were 25.68, 24.75, 20.81, and 22.29 wt.%, respectively. They found that three diffraction peaks, i.e. (002), (101) and (103) indexed to ZnO in addition to the (200) and (220) peaks indexed to MgO which increased as $Mg(NO_3)_2$ concentration increased. They did not report the optical properties of the obtained ZnO:Mg NRs.

Guo *et al.* investigated the effects of the Mg contents (Zn/Mg molar ratios of 1:0, 1:0.25, 1:0.5) on the structural and optical properties of ZnO NRs grown hydrothermally using Mg acetate as a dopant [110]. Their results showed that the films